ISSN 0015-4628, Fluid Dynamics, 2016, Vol. 51, No. 3, pp. 343–359. © Pleiades Publishing, Ltd., 2016.
Original Russian Text © Ya.V. Zagumennyi, Yu.D. Chashechkin, 2016, published in Izvestiya Rossiiskoi Akademii Nauk, Mekhanika Zhidkosti i Gaza, 2016, Vol. 51, No. 3, pp. 48–65.

Unsteady Vortex Pattern in a Flow over a Flat Plate at Zero Angle of Attack (Two-Dimensional Problem)

Ya. V. Zagumennyi[a] **and Yu. D. Chashechkin**[b]

[a]*Institute of Hydromechanics, National Academy of Sciences of Ukraine, ul. Zhelyabova 8/4, Kiev, 03680 Ukraine*

[b]*Ishlinsky Institute for Problems in Mechanics, Russian Academy of Sciences, pr. Vernadskogo 101, Moscow, 119526 Russia*

e-mail: zagumennui@gmail.com, chakin@ipmnet.ru

Received November 2, 2015

Abstract—A technique of self-consistent analytical and numerical modeling of strongly and weakly (with the buoyancy frequency $N = 1.2$ and $0.02\ \mathrm{s}^{-1}$) stratified flows, as well as of almost and absolutely homogeneous flows (with $N = 10^{-5}$ and $0.0\ \mathrm{s}^{-1}$), is developed using the fundamental system of equations without additional hypotheses or constants. Using an open-source software, the basic physical parameters (velocity, density, pressure) and their derivatives in the flow around a thick (0.5 cm) and a relatively thin (0.05 cm) rectangular plate 10 cm long are first calculated within the framework of a unique formulation over a wide range of velocities $0 < U < 80$ cm/s. A complex flow structure comprising leading disturbances, internal waves, vortices, and thin interlayers is visualized. The maximal gradients are observed near the leading edge. In the unsteady vortex regime the structural parameters vary due to the nonlinear interaction of the flow components with different scales. For the finite plate, the calculated friction differs substantially from the Blasius solution but, for a semi-infinite plate, agrees to the accuracy of 5%.

Keywords: strip, numerical simulation, open-source software, stratified fluid, homogeneous fluid, unsteady flow regime, vortices, internal waves.

DOI: 10.1134/S0015462816030066

The studies of the flow past a plate co-directed with the free stream take an important place in hydrodynamics due to the fundamental nature of the problem and important applications. Although the number of publications on the subject is very large, several problems emerged both at the end of the nineteenth century and recently are not still understood. The choice of the shape and thickness of the leading edge of a straight wing is among the most important problems: it was thin in the aeronautical experiments of O. Liliental [1] and thick in the later aeroplane design of the Right brothers, same as in most modern aircrafts.

At present, the flows over a plate and a semi-infinite plane are being studied extensively with the aim to improve the flow laminarization methods [3] and to analyze the structuring mechanisms and the nature of turbulence [4]. In this connection, of a specific interest is the construction of the theory of flows past obstacles without introducing additional hypotheses and relations, and the calculation of physical parameters on its basis, which allows a direct comparison with the experiment.

Due to the mathematical difficulty, from the beginning of the twentieth century the researches started to use approximate models of flows past obstacles and first of all the boundary layer theory [5]. The solution to the problem of a flow over a half-plane, obtained using the assumption of a constant pressure in the direction normal to the wall [6], was used for comparison with experiment and testing numerical models [2, 7] for more than a hundred years.

Later, in calculating the flows of a homogeneous fluid and a compressible gas over a wide range of velocities the asymptotic methods proposed for taking the end effects into account [8] came into practice

under the assumption of a complex multi-deck flow pattern over the body surface [9]. A review of the state-of-the-art of the boundary layer theory with account of its multi-deck structure can be found in [9, 10].

For calculating the vortex flow over a plate, the specific numerical schemes were developed, which simulate the separation and reattachment of the boundary layer [11]. In the experiments carried out in recent years, the "streaky structures" which are transformed into vortex systems downstream were detected in the flow pattern near a plane surface [4, 12, 13].

A new direction of investigations of the flow over a plate is associated with the account for the stratification and diffusion effects. Taking the density variation into account in the system of equations makes it possible to calculate the dynamics and the structure of a number of flows over a wide range of velocities [14]. In a quiescent non-equilibrium medium, the flows compensating the deficiency of matter, caused by the interruption of molecular transport of the stratifying component, arise even near a fixed non-permeable obstacle [15].

Laboratory experiments demonstrated that the fine structural elements in the flows induced by diffusion on an immovable obstacle do not disappear with the beginning of motion, they become even more complex and fine. The fine structural elements are transformed into slow evolving high-gradient interlayers separating internal waves, vortices, and wakes [16].

The calculation of stratified flows at small velocities of the plate is performed using the singular perturbation methods with numerical visualization of the calculated flow patterns. The full asymptotic solution of a linearized problem of the flow past a strip contains two types of functions, namely, the regularly perturbed functions, which describe the weakly attenuating internal waves, and the singularly perturbed functions which describe the high-gradient interlayers near and far from the obstacle [17].

The analysis of the fundamental system of equations within a weakly nonlinear approximation showed that all flow components, both large- and fine-scale, directly interact with each other [14]. The necessity in the simultaneous calculation of the internal waves and the thin transverse band structures observed experimentally [15, 18] impose heavy demands on the mathematical models describing the flows with account for the nonlinear effects.

The development of computer systems and program tools take the mathematical modeling on a new level, comparable in some criteria with the laboratory experiment and full-scale observations in natural conditions. In most papers, the flows are calculated under the assumption of initial homogeneity of the fluid [4, 7], including the case of compressible (barotropic) media [9, 10].

At the same time, the search for the solutions of the problem in the full formulation, with account for the baroclinicity, nonlinearity, and diffusion effects over a wide range of parameters [19] is of scientific and practical interest.

In this article, the results of highly efficient calculations of the flows developing when a plate oriented at a zero angle of attack moves uniformly in both a stratified and a homogeneous viscous incompressible fluid are first presented. The technique developed makes it possible to perform the calculations within the framework of the unique formulation over a wide range of plate lengths and velocities. Using the scale analysis of the system of equations [14], we study an unsteady (transient) vortex regime, which continues our previous studies of stratified flows near an immovable [15] and a uniformly moving horizontal plate in the linear approximation [17].

1. FORMULATION OF THE PROBLEM

We consider a uniform incompressible viscous flow over a rectangular plate. Two situations are considered, namely, the flows of a stratified and a homogeneous fluid. The flows of a strongly stratified fluid, typical of laboratory experiments, and a weakly stratified fluid, typical of natural systems such as ocean and atmosphere, are analyzed separately. The disturbances in a potentially homogeneous fluid (when the inertial effects attributable to the variable density of the fluid can be neglected but a small density gradient makes it possible to retain the completeness of the original formulation) and in the actually homogeneous fluid (the main object of study in theoretical hydromechanics) are also calculated separately.

Table 1

Parameter		Fluids			
		Stratified		Homogeneous	
		Strongly	Weakly	Potentially	Actually
Frequency N, s^{-1}		1	0.02	10^{-5}	0
Linear scales, cm	δ_N^ν	0.1 cm	0.7 cm	31.6 cm	∞
	δ_U^ν	1.25×10^{-4}	1.25×10^{-4}	1.25×10^{-4}	1.25×10^{-4}
	$\delta_N^{\kappa_s}$	3.7×10^{-3}	2.6×10^{-2}	1.2	∞
	$\delta_U^{\kappa_s}$	1.7×10^{-5}	1.7×10^{-5}	1.7×10^{-5}	—

The flows occur in a uniform gravity field with the gravity force acceleration g. The unperturbed exponential density distributions are characterized by the scales $\Lambda = |d \ln \rho_0/dz|^{-1}$, the frequencies $N = \sqrt{g/N}$, and the buoyancy periods $T_b = 2\pi/N$ (their values are given in Table 1).

We consider two-dimensional flows developing over a rectangular horizontal plate with the length $L = 10$ cm and width $h = 0.5$ or $h = 0.05$ cm, immersed in a uniform flow. The leading end of the plate with sharp edges is normal to the horizontal free stream. The obstacle geometry is characterized by the sharpness coefficient $\xi = L/h = 20,\ 200$. We use two right coordinate systems, the first (laboratory) is fitted to the fluid (the z-axis is directed vertically upward) and the second (proper) system is attached to the body, with center being located at the middle of the plate.

The problem is considered in the unique formulation in a wide range of plate velocities $U \in [U_1,\ U_2]$. The diffusion-induced flows over an immovable plate ($U_1 = 0$) were studied in detail in [15]. In this case, on a horizontal plate the vortex cells and the long high-gradient interlayers, adjacent to the sharp edges, are formed. The flows at moderate plate velocities were calculated in the linear approximation in [17].

In the present study, the main attention is focused on the flow with the velocity $U_2 = 80$ cm/s, when the Reynolds number based on the plate length $L = 10$ cm and the viscosity $\nu = 1$ cSt is $\mathrm{Re} = UL/\nu = 8 \times 10^4$, which corresponds to the transitional regime [6]. The calculations are performed for water and a sodium chloride solution, whose density was varied in the range $0.998 < \rho < 1.200$ g/cm^3. The standard density value was $\rho = 1$ g/cm^3.

The mathematical modeling is performed using the fundamental system of mechanics of inhomogeneous incompressible multicomponent fluids, which includes the equation of state of the medium (characterized by the unperturbed distribution of salinity $\rho_0(S_0(z))$, with the density on the central plate horizon ρ_{00}), the continuity equation, the Navier–Stokes equation in the Boussinesq approximation, and the diffusion equation for the stratifying component [19]:

$$\begin{gathered} \rho = \rho_{00}(\exp(-z/\Lambda) + s), \qquad \operatorname{div} \mathbf{v} = 0, \\ \frac{\partial \mathbf{v}}{\partial t} + (\mathbf{v}\nabla)\mathbf{v} = -\frac{1}{\rho_{00}}\nabla P + \nu\Delta\mathbf{v} - s \cdot \mathbf{g}, \\ \partial s/\partial t + (\mathbf{v} \cdot \nabla)s = \kappa_s \Delta s + v_z/\Lambda. \end{gathered} \tag{1.1}$$

Here, s is the perturbation of the salinity (the stratifying component) including the salt compression coefficient, $\mathbf{v} = (v_x,\ 0,\ v_z)$ is the induced velocity, P is the difference of the full and the hydrostatic pressure, $\kappa_s = 1.41 \times 10^{-5}$ and $\nu = 10^{-2}$ cm^2/s are the salt diffusion coefficient and the kinematic viscosity of the solution, t is time, and ∇ and Δ are the Hamilton and Laplace operators. In a more complete formulation, to the system of equations we add the diffusion equation for the visualizing admixture, which is necessary to verify the adequateness of the observations that do not confirm the hypothesis of a 'passive admixture'. Our experiments on the flow visualization showed that the change of the visualizing admixture, a small amount of which cannot affect the dynamics of the process, is accompanied by systematic variations of the flow pattern, whereas the qualitative features of the flow, i.e. the pattern of the admixture concentration, particularly its fine details, depends on the properties of the admixture [14]. The problem is solved in two

steps. In the first step, in a quiescent stratified medium without perturbations we immerse a horizontal plate on which the physically justified initial and boundary conditions are specified in the attached coordinate system [15] (the no-slip conditions on the solid walls and the damping of all disturbances far from the plate). Near the plate, which interrupts the molecular transport of the stratifying component, a diffusion-induced compensatory flow develops, which then is taken as the initial condition for the problem of the flow past the plate:

$$\mathbf{v}|_{t\le 0} = \mathbf{v}_1(x,\, z), \quad s|_{t\le 0} = s_1(x,\, z), \quad P|_{t\le 0} = P_1(x,\, z), \quad v_x|_\Sigma = v_z|_\Sigma = 0,$$
$$\left[\frac{\partial s}{\partial \mathbf{n}}\right]\Big|_\Sigma = \frac{1}{\Lambda}\frac{\partial z}{\partial \mathbf{n}}, \quad v_x|_{x,z\to\infty} = U, \quad v_z|_{x,z\to\infty} = 0, \tag{1.2}$$

where U is the velocity of the uniform free stream and $\mathbf{n}$ is the outward normal on the obstacle surface.

The system of equations and boundary conditions (1.1)–(1.2) is characterized by the set of parameters with the dimensions of length (Λ, L, h) and time (T_b, $T_U^L = L/U$). It contains the dissipative coefficients ν and κ_s entering in the definitions of small dynamic length scales [14].

The large dynamic scales, i.e. the viscous wave scale $\Lambda_\nu = (g\nu)^{1/3}/N$ and the length $\lambda = UT_b$, specify the structure of the attached internal waves [14]. The fine flow structure is characterized by the universal scales $\delta_N^\nu = \sqrt{\nu/N}$ and $\delta_N^{\kappa_s} = \sqrt{\kappa_s/N}$, determined by the dissipative coefficients and the buoyancy frequency (an analogs of the Stokes scale on an oscillating surface $\delta_\omega^\nu = \sqrt{\nu/\omega}$ [19]). Two more scales, i.e. the Prandtl and the Peclet scales, are determined by the dissipative coefficients and the plate velocity: $\delta_U^\nu = \nu/U$ and $\delta_U^{\kappa_s} = \kappa_s/U$. The values of the microscales of the problem for different fluids are given in Table 1.

The ratios of the proper scales of the problem specify the characteristic dimensionless combinations, which include both the traditional Reynolds number $\mathrm{Re}_U = UL/\nu = L/\delta_U^\nu \gg 1$, the internal Froude number $\mathrm{Fr} = U/NL$, the Peclet number $\mathrm{Pe}_U = L/\delta_U^{\kappa_s} \gg \mathrm{Re}_U$, the sharpness coefficient $\xi_p = L/h$ or the space factor $\xi_S = S/h$, where S is the area of the cross section of the obstacle, and the parameters specific for the stratified flows.

The additional dimensionless parameters include the measure scale $C = \Lambda/L$, i.e. the ratio of the buoyancy scale and the body size, and an analog of the inverse Atwood number for continuously stratified media $\mathrm{At}^{-1} = (\rho_1 + \rho_2)/(\rho_1 - \rho_2)$.

The large scales determine the dimensions of the calculation domain, which should contain the structural elements, such as the leading disturbances, the wake, the waves, and the vortices, whereas the microscales determine the cell size and the time step. For low velocities of the plate, the Stokes microscales are critical, and for large velocities the Prandtl scales are critical.

2. NUMERICAL MODELING OF THE PROBLEM

The numerical solution of the system of Eqs. (1.1) with boundary conditions (1.2) was constructed using the OpenFoam package [20] with the open original code, in which we designed the 'stratifiedFoam' solver. This solver realized numerically the mathematical model using a finite-volume method. The package designed for calculating 3D problems makes it possible to calculate 2D problems by the creation of an additional calculation cell in the third dimension and the specification of 'empty' boundary conditions on the side edges of the calculation domain.

To take into account the stratification and diffusion effects, the standard 'icoFoam' solver for the unsteady Navier–Stokes equations in uniform fluid was supplemented with the new variables (the density ρ and the salinity perturbation s) and the corresponding equations for their calculation. We also added the new auxiliary parameters (the buoyancy frequency and scale: N and Λ; the diffusion coefficient κ_s; the gravity force acceleration g; and others). In the Navier–Stokes equation for the vertical velocity component, we added the terms responsible for the action of the buoyancy force, and in the diffusion equation the terms characterizing the background stratification. The no-flow boundary conditions for the normal gradient of

the salinity perturbation, specified on the entire impermeable surface of the plate, are realized numerically using original computer codes based on the extended utilities and libraries of the OpenFoam package.

To interpolate the convective terms, we used a TVD-scheme with a limiter, which introduced a minimal numerical diffusion and ensured the absence of solution oscillations. For the finite-difference approximation of the time derivative, we used a second-order implicit asymmetric three-point scheme with the backward differences, which ensured a good time resolution of the physical process.

With the aim to minimize the calculation time, the grid was generated using the extended utilities of the OpenFoam package, which made it possible to distinguish and locally decrease the grid cells in subdomains with account for the problem scales and to reduce the total number of the grid cells to 10^6, retaining the high spatial discretization of high-gradient flow regions. The parallel calculations were performed using the supercomputer complex of the Research Computational Center of the Lomonosov Moscow State University and the UniHUB technological platform which provided a direct access to the calculation segment of the MSTs RAS cluster.

The calculations were finished when the calculated integral flow parameters or their statistical estimates went on their values for the steady-state regime. The sizes of the grid cells were chosen from the condition of the adequate resolution of fine-structure flow elements, associated with the stratification and diffusion effects, which imposed the substantial restriction on the minimal spatial step: in the high-gradient flow regions, at least several grid cells should fall on the minimal linear scale (see Table 1).

The control of the calculation accuracy was performed by the specification of an admissible error in the solution of the resultant system of linear algebraic equations, which was found by the PCG and PBiCG iteration solvers using the methods of conjugate and bi-conjugate gradients with a preconditioner based on the DIC and DILU procedures. The final accuracy of the calculations was 10^{-6} for the pressure field and 10^{-10} for the other parameters. The stability of the non-stationary calculations was ensured by the choice of the time step from the Courant condition $\mathrm{Co} = |\mathbf{v}|\Delta t/\Delta r \leq 1$, where Δr is the grid cell size, and $|\mathbf{v}|$ is the local flow velocity. The additional control was ensured by the comparison of independent calculations for different liquids.

3. THE CALCULATION RESULTS

The initial state of the non-equilibrium stratified medium near an impermeable obstacle is characterized by the diffusion-induced circulatory flows [17, 18]. The typical pattern of the vertical velocity component near an immovable impermeable horizontal plate in the exponentially stratified medium is shown in Fig. 1a ($N = 1.2$ s^{-1}, $L = 10$ cm, $h = 0.5$ cm). For convenience of printing, the original color images were transformed into the black and white images: for the positive values, the grey color tones vary from grey to dark-grey, and for negative values from dark-grey to black.

The maximal value of the flow velocity (about 4 μm/s) is attained near the plate corners and the lengths of horizontal layers adjacent to the edges are more then 4-fold greater than the plate length. With increase in the fluid density gradient, the height of the cells increases and the fluid circulation intensity decreases. For small stratifications, the velocity of the circulating motion becomes negligibly small, and in the homogeneous fluid approximation this kind of motion is absent at all [14, 15].

As the plate comes into motion in a stratifies fluid, the patterns of the parameters change cardinally: the symmetry is lost, the leading disturbances ate formed, and the attached waves and the lee wake appear [16–18]. The typical flow patterns presented in Figs. 1b–1d illustrate the evolution of the vertical velocity field in the plane (x, z) with increase in the plate velocity (the flow established after the finish of the rapid transient processes associated with the beginning of the plate motion).

At small Reynolds numbers ($\mathrm{Re} < 10^3$, Fig. 1b), the leading disturbances and the attached internal waves generated by the edge singularities at the plate corners are clear expressed in the flow, as in the linear analysis [17]. In a typical interference pattern, the internal waves with the wavelength $\lambda = 5.2$ cm are formed in the counter-phase near the leading and trailing edges, and at the middle of the plate the interference damping of wave disturbances occurs.

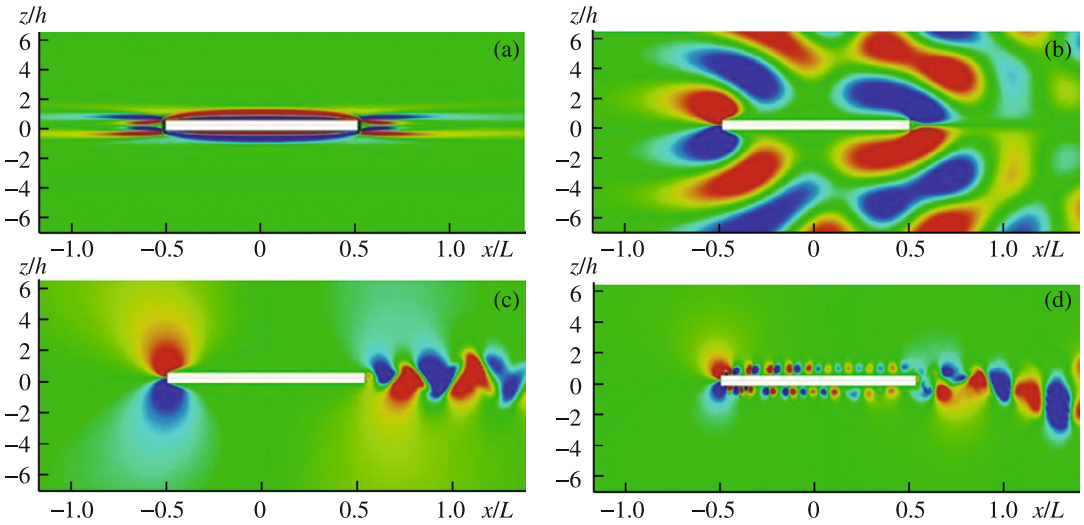

Fig. 1. Vertical-velocity pattern near a plate in a stratified fluid ($N = 1.2$ s^{-1}, $L = 10$ cm, $h = 0.5$ cm): (a) diffusion-induced flow ($U = 0$); (b–d) uniform motion with the velocity $U = 1.0$, 5.0, 80 m/s, Re = 1000, 5000, 80000; Fr $= U/NL_x = 0.1$, 0.5, 6.7; $\lambda = UT_b = 5.2$, 26, 418 cm.

The lines of maximal disturbances in the waves are inclined at an angle of about 35° to the horizon. The maximal value of the vertical velocity (0.56 cm/s) is attained at the distance $\Delta x = 0.06$ cm from the leading edge of the plate, and the weaker extremum $v_z = 0.14$ cm/s is registered at the distance $\Delta x = 0.7$ cm from the trailing edge.

The maximal values of the horizontal velocity component v_z are more than 1.5-fold greater than the free-stream velocity. They are localized along the line of maximal disturbances, the distance from which to the plate surface decreases downstream from 2 cm at the region ahead of the leading edge of the plate to 1 cm near the trailing edge. The minimal value $v_x \approx -0.07$ cm/s is attained in the wake region at the central horizontal plane of the plate at a distance of 0.35 cm from the trailing edge.

At moderate Reynolds numbers (Re $= 5 \times 10^3$, Fig. 1c), the length of the internal waves is greater ($\lambda_i = 26$ cm) and the phase surfaces go outside of the visualization region. Here, the dominant elements are the compact vortex structures generated at the leading edges, where the excess stagnation pressure ahead of the body changes into the rarefaction in the regions with large vertical velocities in the divergent flow, and simultaneously large density gradient disturbances are formed.

It is near the leading edge where the main generation of vorticity $\mathbf{\Omega} = \operatorname{curl} \mathbf{v}$ occurs, with the vorticity generation rate being determined, as follows from the Bjerknes theorem [21], by the non-collinearity of the vectors of the pressure ∇P and the density $\nabla\rho$ gradient: $d\mathbf{\Omega}/dt = \nabla P \times \nabla(1/\rho)$. The second region of the generation and restructuring of the vortices shedding to the wake is the convergent flow near the trailing edge.

The extremum values of the vertical velocity disturbances, which amount to $v_z \approx 4$ cm/s in modulus, are observed at a distance of 0.05 cm from the upper and lower sharp edges of the plate. Much smaller values $v_z \leq 1.4$ cm/s are observed in the lee wake, in the regions of localized vortex structures.

At the distance $\Delta x \approx 0.25$ cm downstream from the leading edge, on the horizon $\Delta z \approx 0.4$ cm of the plate surface the maximal disturbances of v_x are observed, which exceed the free-stream velocity by not more than 10%. Almost similar extremum values of v_x are detected in the wake vortex structures. The minimal value of the horizontal velocity, equal to $v_x \approx -0.045$ cm/s, is observed in the central horizontal plane in the wake behind the plate at a distance of 0.5 cm from the trailing edge.

The maximal values of the vorticity $\mathbf{\Omega} = \operatorname{curl} \mathbf{v} \approx 120$ s^{-1} are localized near the lower leading edge, and the minimal values near the upper edge. Near the trailing edge, the vorticity values are much smaller (~ 25 s^{-1}), and in the nearest vortices the vorticity is even smaller (~ 14 s^{-1}). With increase in the distance from the plate, the vorticity starts to decrease sharply, and at the distance $\Delta x = L$ from the trailing edge the vorticity is not greater than 2 s^{-1}.

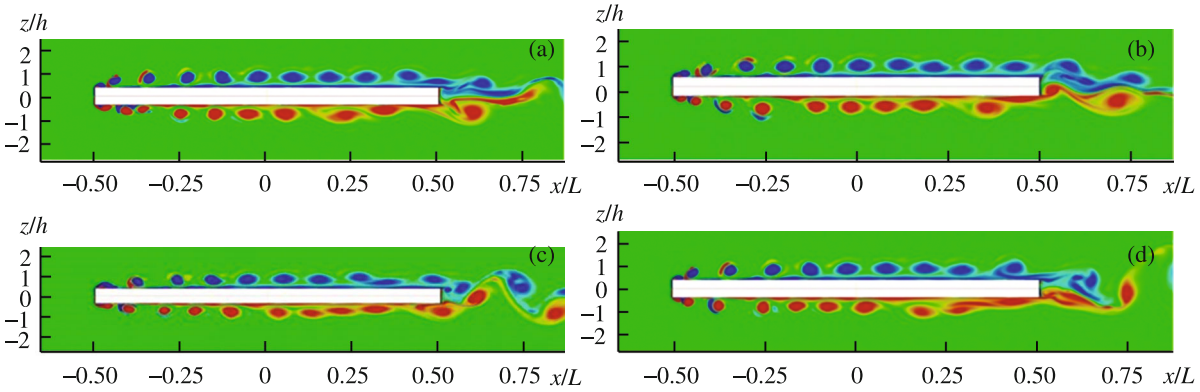

Fig. 2. Time evolution of the vorticity field in a stratified flow over a plate ($N = 1.2$ s^{-1}, $L = 10$ cm, $h = 0.5$ cm, $U =$ 80 cm/s, Re = 80000, Fr = 6.7): (a–d) $t = 2.0$, 2.025, 2.05, and 2.07 s.

Of a practical interest is the unsteady flow pattern at large Reynolds numbers $\mathrm{Re} = 8 \times 10^4$, when together with the large eddies small eddies are formed in the neighborhood of the leading edges (Fig. 1d). All flow components actively interact with each other [14], with the fine structures and even with the attached internal waves, the length of which in this case is much greater than the dimensions of the observation domain [16–18]. Multiple interactions of the flow components having different scales are manifested in the unsteadiness of the flow even at the stationary boundary conditions.

As can be seen in the prepared video, the vortices are partially drifted from the region near the leading edge, where they are formed, and transported by the flow along the upper and lower surfaces of the plate. The vortices reach the separation region near the trailing edge at different instants of time. The variability of the location and the intensity of the shedding vortices result in the deviations of the wake axis from the horizon and in the oscillations of the lee flow structures.

The unsteadiness of vortex structures developing at $U = 80$ cm/s is illustrated by the successive vorticity patterns $\Omega_y = \partial v_X/\partial z - \partial v_z/\partial x$ during the time interval of 0.75 s, shown in Fig. 2. In the black and white images of the vorticity fields, the negative values of the vorticity (with the counter-clockwise rotation) correspond to the grey tones, and the positive values (clockwise rotation) to the dark-grey tones.

The typical dimension of the core of the vortex filaments, shown in Fig. 2, in which the fluid above the plate rotates clockwise and below the plate counter-clockwise, is $\lambda_p \approx 0.35$ cm. With approach to the trailing edge of the plate, the shape of the vortex elements slightly changes: the vortices are elongated in the outer-flow direction, with the distance between the centers of the neighboring vortices being almost identical and equal to $d_p \approx 1$ cm. In the wake behind the plate, the dimensions of the vortex structures slightly increase to $\lambda_w \approx 0.54$ cm, and the distance between the centers of the neighboring vortices increases to $d_w \approx 2.4$ cm.

The vorticity decreases in the vortex cores as the vortices travel along the plate. In the first vortex, the vorticity is about 2500 s^{-1} and in the last less than 450 s^{-1}, i.e. the vorticity decreases in more than five times. However, directly behind the trailing edge of the plate, in the wake region the vorticity again increases sharply to the values of more than 1200 s^{-1} and then decreases downstream to the value of 120 s^{-1} at a distance equal to the plate length from the trailing edge.

It should be noted that several first vortex cores near the leading edge are partially covered with thin interlayers with the vorticity of opposite sign. The variability of the shape and location of these interlayers is one more manifestation of the structural complexity of the unsteady flow pattern near a finite-length plate at the stationary boundary conditions.

The analysis of the video films consisting of the groups of successive patterns of physical parameters, calculated with an interval of 0.01 s (equivalent rate is 100 frames/s), indicated that the vortices formed near the leading edge are transported by the flow independently along the upper and lower plate surfaces with the phase velocity $C_p \approx 0.6U$, and then the vortices meet together in the wake behind the plate. The average local vortex formation frequency on the plate sides can be calculated using the formula: $\omega_p = C_p/d_p \approx 52$ Hz.

The interaction of the unsteady merging streams generates complex multiscale structures adjacent to the trailing edge. However, even at a distance of 0.8 cm (of the order of two vortex elements) the flow pattern becomes more regular and typical of vortex flow behind an obstacle with rectangular shapes. In the wake behind the plate, a typical vortex street is formed. In this street, the frequencies of local flow oscillations, which are smaller than directly above the plate, do not exceed the limiting for these conditions value $\omega_w \approx 22$ Hz.

Both groups of intense vortices are generated in the regions of co-existence of flow components with different dimensions, which co-exist also in the linear models, namely, the edge singularities near the plate edges and the large internal waves [14]. The new structural elements, i.e. the vortices, interact with the free stream and start to move downstream when their value reaches a critical value. Then a new vortex starts to grow in the vacant place.

One advantage of our approach is the possibility to calculate simultaneously different physical quantities, both those entering in the fundamental system of equations (velocity v, density ρ, pressure P) and the derivatives, including the vorticity $\mathbf{\Omega}$, and the baroclinic vorticity generation rate $\dot{\mathbf{\Omega}}$, the components of the pressure and density gradients (($\partial P/\partial x_i$ and $\partial \rho/\partial x_i$), and the dissipation rate of the mechanical energy ε.

The instantaneous patterns of different fields in the vertical plane passing through a streamline of the unperturbed flow in the strongly stratified ($N = 1.2$ s^{-1}, Fr $= 6.7$) and the potentially homogeneous fluid ($N = 10^{-5}$ s^{-1}, Fr $= 8 \times 10^5$) are shown in Figs. 3 and 4. Despite the general similarity in the vortex flow structures near the uniformly moving plate ($U = 80$ cm/s, Re $= 8 \times 10^4$), each flow field is characterized by its own geometry and scales of the elements.

In the flow patterns in the strongly and weakly stratified fluids shown in Fig. 3, there are a number of structural flow elements, both large-scale (leading disturbances, vortices, and internal waves) and small-scale, which in the linear model of the flow are described by the regularly and singularly perturbed functions, respectively [17].

In the field of the horizontal velocity component ahead of the plate, in both fluids the retardation of the fluid, typical of the blocking region at small velocities of the body [18], is expressed only slightly. The velocity deficiency region above and below the plate is an analog of the boundary layer with imbedded flow stagnation zones in the vortex cores (in the black and white images, the positive values of the field correspond to the grey tones and the negative values to the dark-grey tones). This region is surrounded by the layer of the high-velocity fluid, formed by the summation of the velocities of the free stream and the outer edges of the vortex structures.

Qualitatively, the flow patterns in the strongly and weakly stratified fluids are fairly similar, a slight difference is only in details: nine vortex cores and a more pronounced trailing vortex in the strongly stratified fluid against eight vortex cores and an oscillating wake in the weakly stratified fluid. A smoother boundary of the retardation flow region can be explained by the buoyancy force effect which damps the vertical displacements.

In the vertical-velocity patterns, the leading disturbance is expressed even more clear. The further analysis of the video film indicated that the asymmetry of the spots ahead of the body in the strongly stratified fluid is the result of the unsteadiness of the flow. The shape of these spots varies with time. In the image shown, where each vortex is represented by the pair of spots with opposite flow directions, the stratification effect is expressed more clear.

The attenuation rate of nonuniformities in the strongly stratified fluid is greater than in the weakly stratified fluid, the vortex structure of the wake has a smaller scale and the outer boundary is smoother. The splitting and the turn of the flow near the leading edge, same as the merging behind the plate, result in the formation of regions with an excess and a deficiency of the pressure, which affect the drag force. In the wake, there are large-scale vortex elements.

Of a specific interest are the fields of the baroclinic vorticity generation rate, the values of which are determined by the pressure and density gradients: $\dot{\mathbf{\Omega}} = \nabla P \times (\rho^{-1})$. In the pattern of this quantity, the most complex and irregular in the flows of inhomogeneous fluids, near the leading edge there are both the generation (above and below the edge) and dissipation (ahead of the body) regions, which have the size of

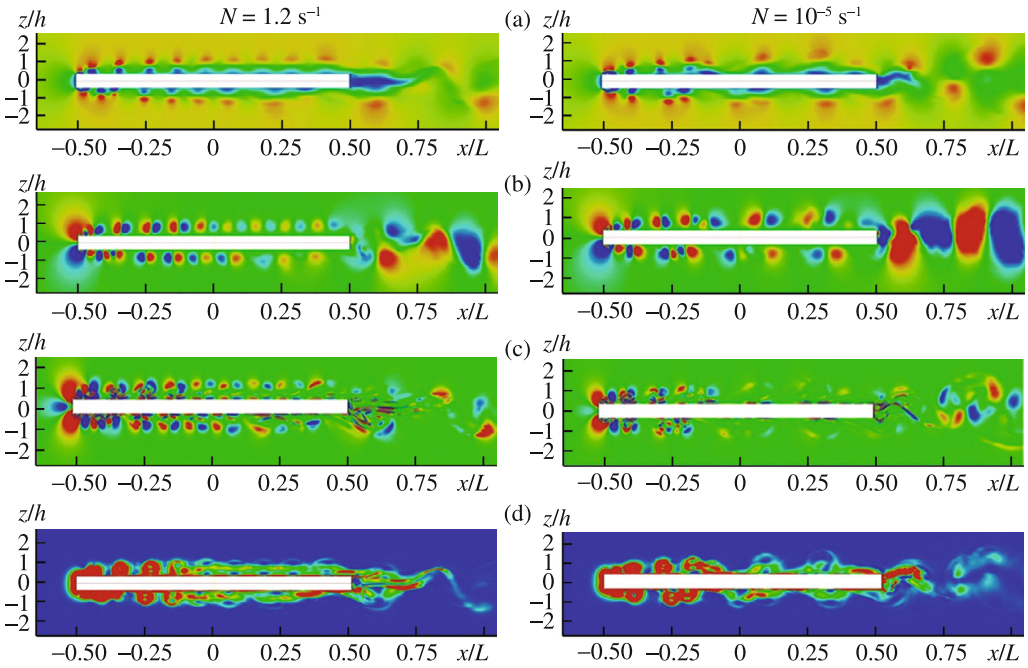

Fig. 3. Instantaneous patterns of parameters near the plate ($L = 10$ cm, $h = 0.5$ cm, $U = 80$ cm/s, $\mathrm{Re} = 8 \times 10^4$) in the stratified (left column, $N = 1.2$ s^{-1}, $\mathrm{Fr} = 6.7$) and the potentially homogeneous fluid (right column, $N = 10^{-5}$ s^{-1}, $\mathrm{Fr} = 8 \times 10^5$): (a, b) horizontal v_x and vertical v_z velocity components, (c) baroclinic vorticity generation rate $\dot{\Omega}_y$, (d) dissipation rate of mechanical energy ε.

the order of the plate thickness. Downstream, the structures become thinner and, in addition to the remnants of the vortex elements, multiple thin regions of the enhancement and break-up of the vorticity arise, which are slowly elongated.

Behind the trailing edge in the wake there are predominantly thin stripped structures, which on the average are oriented streamwise and are deformed by large-scale nonuniformities. In the strongly stratified fluid, the disturbances of both signs are observed over the entire length of the plate and, in the weakly stratified fluid, only over the first one quarter. In the wake behind the body, in the zones of interaction between the wake vortices and the outer stream there are the regions of both vorticity generation and dissipation. The geometry of this parameter illustrates the dynamics of the formation of fine structures in vortex flows and the mechanism of splitting of the flow patterns into banded structures observed in the schlieren images of stratified flows [22].

The dissipation rate of the mechanical energy $\varepsilon = 0.5\rho\nu(\partial v_i/\partial x_k + \partial v_k/\partial x_i)^2$ is nonzero only in a fairly narrow blocking zone, where the horizontal stream is deflected moving around the plate. This parameter attains the maximal values in the vortex structures over the first one third of the plate length. In a weakly stratified fluid, the dissipation regions over the second half of the plate length turn out to be larger than in the strongly stratified fluid. It should be noted that there is a qualitative difference between the vorticity generation rate pattern, in which the fine structures are expressed (Fig. 3c), and the fairly smooth energy dissipation rate pattern (Fig. 3d).

The complication of the patterns of the gradient components in Fig. 4 is attributable to the properties of differential operators generating two groups of spots for each vortex core: one group corresponds to the disturbance growth regions, and the second to the disturbance attenuation regions. At the same time, the advantage of the patterns of the component gradients is a more complete visualization of the structural details, which makes it possible to identify small-scale elements against the background of larger elements.

In the distribution of the horizontal component of the pressure gradient $\partial P/\partial x$, an array of spots with different signs is clear, same as in the vertical-velocity pattern (Fig. 3b). In the distribution of the vertical component $\partial P/\partial z$, there is a more rarefied array of vertically located spots of different color. Here, the vortices are well resolved, in particular, in Fig. 4a over the plate there are ten cores, which is greater by one

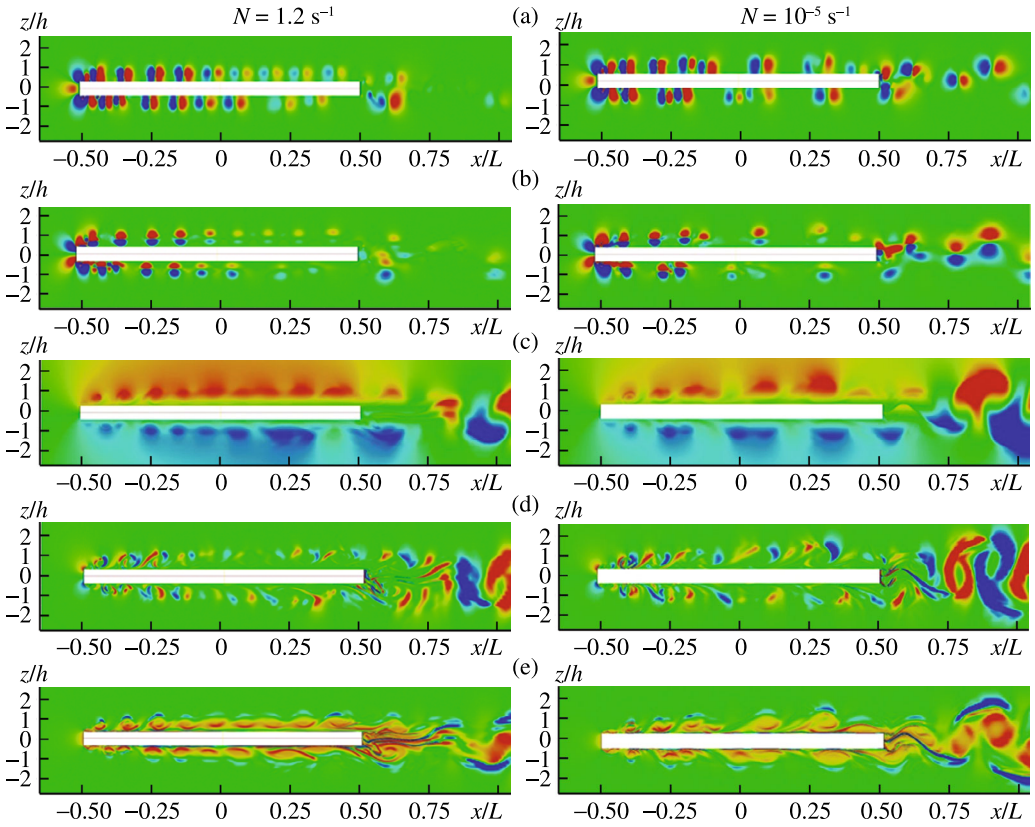

Fig. 4. Instantaneous patterns of parameters near the plate ($L = 10$ cm, $h = 0.5$ cm, $U = 80$ cm/s, $\mathrm{Re} = 8 \times 10^4$) in the stratified (left column, $N = 1.2\ \mathrm{s}^{-1}$, $\mathrm{Fr} = 6.7$) and the potentially homogeneous fluid (right column, $N = 10^{-5}\ \mathrm{s}^{-1}$, $\mathrm{Fr} = 8 \times 10^5$): (a, b) horizontal $\partial P/\partial x$ and vertical $\partial P/\partial z$ components of the pressure gradient, (c) density disturbance $\rho_d = \rho - \rho_0$; (d, e) horizontal $\partial \rho_d/\partial x$ and vertical $\partial \rho_d/\partial z$ components of the density gradient.

than in the horizontal velocity pattern. Even more complicate flow pattern is resolved near the leading edge. In a weakly stratified fluid, the disturbances degenerate more slowly as compared to the strongly stratified fluid and the scale of vortex structures is noticeably smaller (Fig. 4a).

In the density disturbance pattern $\rho_d = \rho - \rho_0$, a flow region expanding with the distance from the leading edge is clear expressed. This region is bounded by the lower edges of the spots of the partially mixed fluid in the vortices (Fig. 4c). Above the plate, the layer with increased values is located above the plate and the layer with decreased values is below the plate, which is attributable to the transport of the fluid by the vortices drifting from the equilibrium horizons. The number of compact elements in the density pattern in the weakly stratified fluid is noticeably smaller than in the strongly stratified fluid. Near the trailing edge of the plate, there are regions where the density field is disturbed only slightly.

The patterns of the density gradient component (Figs. 4d, 4e) compliment the density pattern. In the field of the horizontal component of the density gradient, thin layers of both signs, localized on the vortex shells, are well expressed. Behind the body they are combined in compact spots. In the weakly stratified fluid, the structures of the vertical component of the density gradient are oriented mostly horizontally and form its own system of spiral curls, typical of vortex elements. The local patterns of different physical quantities in the wake in Fig. 4c–4e differ substantially and the locations of the centers of the regions which they trace do not coincide with each other.

It should be specially noticed that the geometry and the fine structure of the fields of the pressure and density gradients, which determine the spatial and temporal variation of the kinematic parameter, i.e. the vorticity generation rate and hence the variation of the vorticity itself, are different.

All instantaneous flow patterns and the vorticity patterns in Fig. 2 are in continuous evolution. The variation of the velocity pattern in the kinematic description is attributable to the generation and break-up of

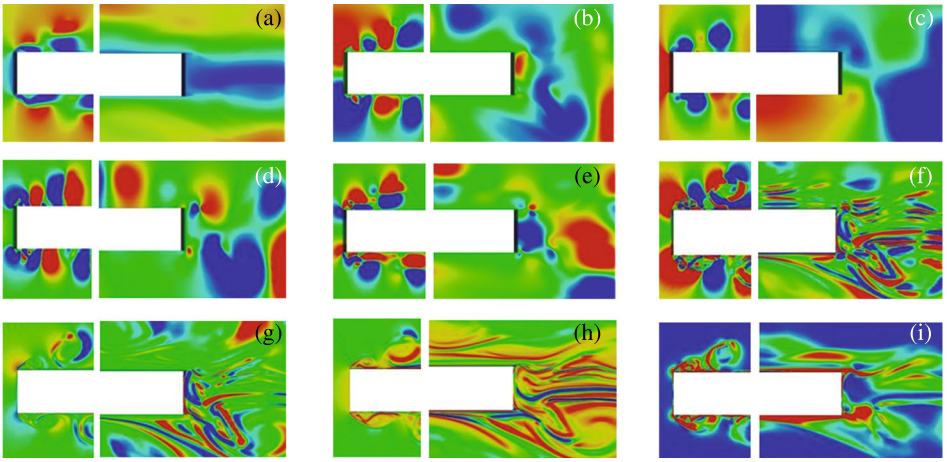

Fig. 5. Fine structure of the fields near the leading and trailing edges of the plate ($N = 1.2\,\mathrm{s}^{-1}$, $L = 10\,\mathrm{cm}$, $h = 0.5\,\mathrm{cm}$, $U = 80\,\mathrm{cm/s}$, $\mathrm{Re} = 80000$, $\mathrm{Fr} = 6.7$): (a, b) horizontal v_x and vertical v_z velocity components; (c–e) pressure P, horizontal $\partial P/\partial x$ and vertical $\partial P/\partial z$ components of the pressure gradient; (f) baroclinic vorticity generation rate $\dot{\Omega}_y$; (g, h) horizontal $\partial \rho_d/\partial x$ and vertical $\partial \rho_d/\partial z$ components of the density disturbance gradient; (i) dissipation rate of the mechanical energy ε.

new elements (vortices) due to the non-synchronized variation of the physical parameters of thermodynamic nature, in particular, the density and pressure gradients [21].

In the dynamic description, the generation of new elements with their own kinematics and spatial and temporal scales is associated with the high order and nonlinearity of the fundamental system of equations [14]. Even in the linear approximation, the complete solutions of this system contain several functions [17] which, in the nonlinear models, are corresponded by the components interacting with each other and generating new types of disturbances [14].

The zoomed images illustrate the substantial difference in the behavior of the patterns of the physical parameters in the divergent flow with large pressure gradients ahead of the plate and in the convergent flow behind the plate (Fig. 5).

The horizontal-velocity pattern is most simple, the deficiency of this velocity is manifested in a thin layer over the entire contour of the obstacle, in the vortex cores, and in the wake (Fig. 5a). In a more complex pattern of the vertical velocity, one can see a leading disturbance, a complex system of vortex cores with different sizes near the leading edge, and large vortices of irregular shape in the wake (Fig. 5b). Highly organized structures are observed in the pressure field: the excess values in the stagnation region ahead of the body, compact regions of the deficiency in the vortex cores, the excess in the zones of contact of the impinging flows with the plate surface, and irregular large-scale variations near the trailing edge and in the near wake (Fig. 5c).

The scale of the smooth spots in the pressure gradient patterns increases with increase in the distance from the leading edge and attains the maximum in the wake, where the shape of the spots is specific for each component (Figs. 5d, 5e).

A sharp structure of the multiscale pattern of the baroclinic vorticity generation rate illustrates the efficiency of the Bjerknes mechanism in the wake flow region (Fig. 5f). The thin-layered pattern with large variations of this parameter near the trailing edge is the indication of the smaller efficiency of generation and an increase in the scales of the structural elements due to the damping action of viscosity (see Fig. 2). The main process of vortex formation occurs in the neighborhood of the leading edge, where the pressure and density gradients are maximal.

The layered structures with the smallest scales are observed in the patterns of the density gradient, which is due to the small ratio of the diffusion and kinematic viscosity coefficients (Figs. 5g, 5h). The difference in the structures of the pressure (Figs. 5d, 5e) and density (Figs. 5g, 5h) gradients ensures the efficiency of baroclinic generation of vorticity in dynamically complex flow fields, containing the large-scale (internal waves and vortices) and fine-scale components.

Table 2

	Stratified fluid, $N = 1.2\ \mathrm{s}^{-1}$		Potentially homogeneous fluid, $N = 10^{-5}\ \mathrm{s}^{-1}$		Localization
Field	Minimum	Maximum	Minimum	Maximum	
U_x, m/s	-1.07	1.83	-1.058	1.502	LE, VS
U_z, m/s	-0.89	0.98	-0.995	0.914	LE, VS
P, Pa	-1276	322	-1108	333	LE, VS
$\partial P/\partial x$, Pa/m	-2.8×10^6	1.12×10^6	-2.3×10^6	0.91×10^6	LE, VS
$\partial P/\partial z$, Pa/m	-2.5×10^6	2.1×10^6	-2.1×10^6	2.0×10^6	LE, VS
ρ_d, kg/m^3	-2.6	3.8	-1.68×10^{-10}	1.8×10^{-10}	WE, IF
$\partial \rho_d/\partial x$, kg/m^4	-1900	2700	-2.7×10^{-10}	-3.4×10^{-10}	TE
$\partial \rho_d/\partial z$, kg/m^4	-3100	1450	-2.53×10^{-10}	-1.58×10^{-10}	IF
$\dot{\Omega}_y$, s^{-2}	-2.9×10^8	5.5×10^8	-0.028	0.036	LE, TE, IF
ε, kg/m s^{-3}	0	1.1×10^6	0	0.94×10^6	LE, VS

Notation: IF—high gradient interfaces, LE—leading edge, TE—trailing edge, VS—vortices, WE—wake.

The zoomed image makes it possible to identify the complex structure of a fairly compact field of the dissipation rate of mechanical energy ε which reflects the integral dissipative action of all structural elements (Fig. 5j).

The typical values of the calculated physical parameters are given in Table 2.

In general, it is worth to note the differences in the field structures associated with the independency of the physical parameters in the fundamental system. In the vortex flow near the plate, in the neighborhood of the leading edge the positive variations of the horizontal velocity attain 80% of the free-stream velocity. The negative variations are even greater (in absolute value), and with increase in stratification the difference increases. In this regime, the variations of the vertical velocity, increasing with the decrease in stratification, are even greater than the free-stream velocity due to the action of the nonuniform buoyancy forces.

The maximal variations of the density and its gradient, formed as a result of the superposition of all dynamic disturbances violating the initial stratification, are observed near the trailing edge and in the wake behind the body. In a weakly stratified fluid, their values lie beyond the limits of sensitivity of the existing measuring methods; however, the computer resources and the numerical methods make it possible to track the geometry of high-gradient regions and estimate the baroclinicity effect on the flow structure and the vorticity generation.

Of a particular research and practical interest are the results of calculating the pressure field, on which noticeable restrictions are imposed in the traditional description [5, 10, 12]. It may be noted qualitatively that the stratification affects the flow field only slightly, while the transverse dimension of the obstacle produces a strong impact, which is observed experimentally [16, 18].

In all patterns shown in Fig. 6, we see a pressure increase in the leading disturbance ahead of the plate, strong rarefaction spots in the divergent flow near the leasing edge, and a pressure deficiency in the regions of localization of vortex elements. For the fixed other parameters, the vortex size depends on the plate thickness: for a thin plate, they take the form of vortex filaments; for a thick plate, they look like crosswise bands, as those observed experimentally [18].

The temporal analysis of the video films showed that, for a thick plate, the formed vortices with the diameter $\lambda_p \approx 0.35$ cm separate from the leading edge, roll downstream along the plate with the velocity $C_p \approx 0.6U$ and then are shed into the wake, forming a traditional vortex street with the element size $\lambda_w \approx 0.54$ cm. Meanwhile, in the flow over a thin plate the compact crosswise bands (with the thickness $\mu_p \approx 0.08$ cm and the average distance between the neighboring structures $\delta_p \approx 0.32$ cm) travel downstream with the smaller velocity $C_p \approx 0.45U$ and are almost completely damped over a one fourth part of the plate length.

The second group of the thicker crosswise bands with $\mu_w \approx 0.17$ cm and the step $\delta_w \approx 0.5$ cm is formed

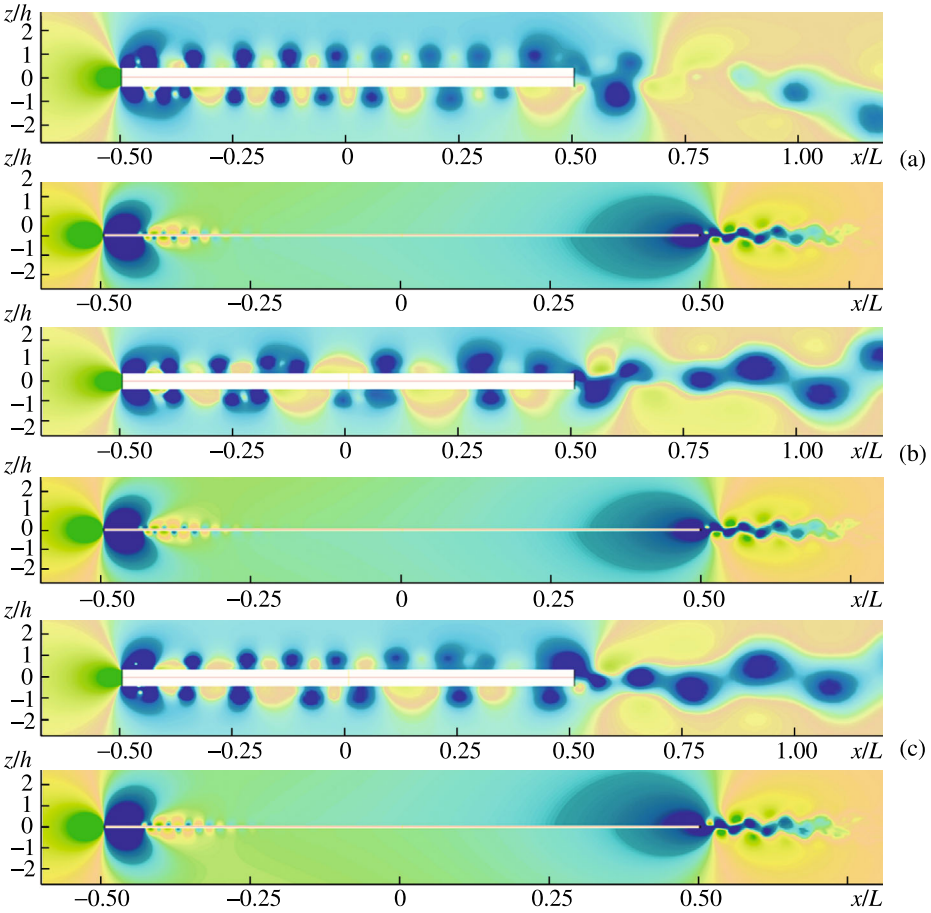

Fig. 6. Pressure fields over horizontal plates ($L = 10$ cm, $h = 0.5$ and 0.05 cm, $U = 80$ cm/s): (a, b) $N = 1.2$; 10^{-5} s; (c) actually homogenous fluid $N = 0$.

behind the trailing edge and is damped on the same length in the wake. The values of the local frequency of vortex generation on both sides of the plate and in the wake, calculated using the formula $\omega_{p,w} = C_p/\delta_{p,w}$, amount (on the average) to about 110 and 72 Hz, respectively. The crosswise banded structures were observed earlier in the schlieren photographs of the stratified flow around a thin plate [16, 18].

The average profiles of the dimensionless pressure and longitudinal velocity in different crosswise sections located at the distances from the leading edge, multiple to one quarter of the plate length, are shown in Fig. 7 (in the insertions, we show the zoomed initial segments of the curves). The averaging was performed over the interval $\Delta t = 1$ s, starting from a certain instant after the beginning of the plate motion with a constant velocity. This instant was taken as the real beginning of the established flow regime with oscillations (here, this instant was about 2 s). On the upper edge of the plate, we set $z = 0$ and the marginal sections are remote from the ends by the distance of 1 mm.

The average pressure distributions vary nonmonotonically in a layer with the thickness of about $\Delta_p \approx 4 \times 10^3 \delta_U^\nu = 0.5$ cm, adjacent to the plate surface, and then tend asymptotically to the unperturbed values in the free stream (Fig. 7a).

The maximal pressure variations are observed in the neighborhood of the leading edge of the plate as a result of the intense vortex generation effect. The negative value of the pressure, which directly on the wall is $P_{pl} = -1.28P_0$, continues to decrease in a layer with the thickness $\Delta_P^{\min} \approx 4 \times 10^2 \delta_U^\nu = 0.05$ cm to its minimum $P_{\min} = -1.6P_0$, after which it starts to increase and tends to its unperturbed value.

With increase in the distance of the section from the leading edge, the pressure variations decrease, the points of maximum move father from the plate surface, and the pressure value on the plate tends to its unperturbed value. The exclusion is only the region near the trailing edge of the plate, where the aver-

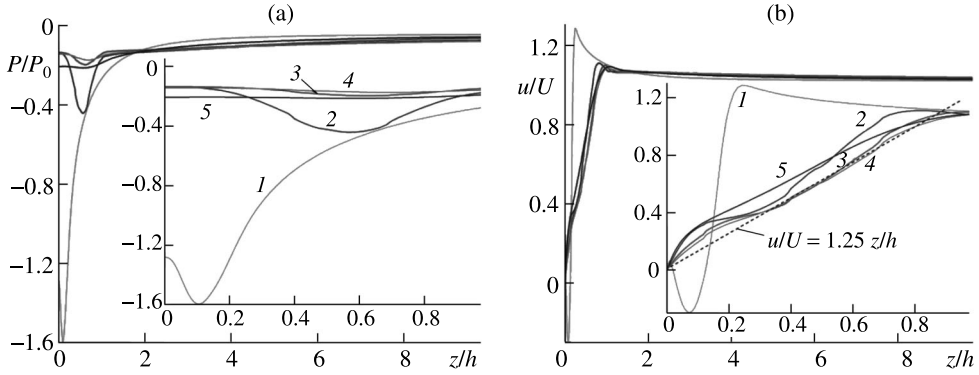

Fig. 7. Average profiles of the pressure and velocity in different sections ($N = 1.2\ \mathrm{s}^{-1}$, $L = 10$ cm, $h = 0.5$ cm, $U = 80$ cm/s, Re = 80000, Fr = 6.7): (a, b) pressure and longitudinal velocity component, curves (*1–5*): $x/L = -0.5, -2.5, 0, 0.25, 0.5$.

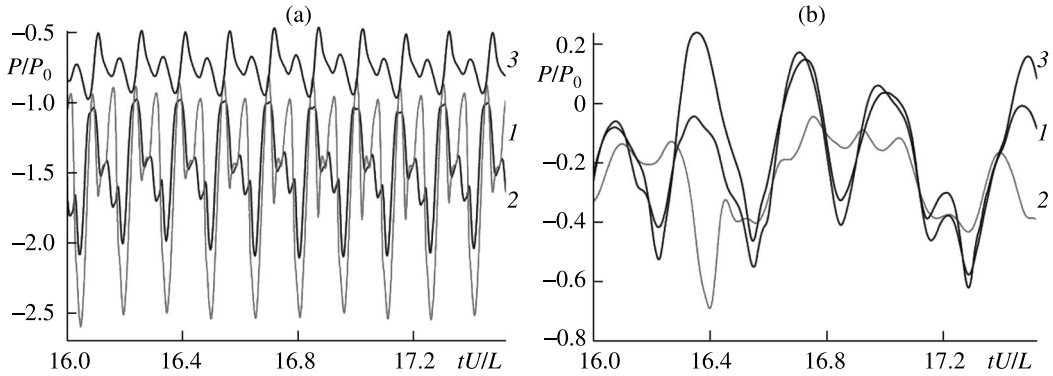

Fig. 8. Time evolution of the normalized pressure at different distances Δz from the upper surface of the plate ($N = 1.2\ \mathrm{s}^{-1}$, $L = 10$ cm, $h = 0.5$ cm, $U = 80$ cm/s, Re = 80000, Fr = 6.7): (a, b) above the leading and trailing edges, curves (*1–3*): $\Delta z = 0.02$, 0.05, and 0.2 cm.

age pressure again drops sharply, both on the plate surface and in the near-wall region with the thickness $\Delta_P < 3 \times 10^3 \delta_U^\nu$, which is attributable to effect of wake vortices.

The distribution of the longitudinal velocity component across the flow near the leading edge differs noticeably from the profiles in other sections considered. In the layer with the thickness $\Delta_u \approx 3.2 \times 10^3 \delta_U^\nu$, the velocity increases almost linearly by the law $v_x/U = 1.25z/h$, then it sharply increases to the maximal value $v_x \approx 1.1U$ and after that tends asymptotically to the free-stream velocity (Fig. 7b).

Near the leading edge, the disturbances of the longitudinal velocity attain the minimum $v_x^{\min} \approx -0.3U$ at the distance $\Delta_U^{\min} = 3 \times 10^2 \delta_U^2$ from the plate surface and then change the sign and increase to $v_x^{\max} \approx 1.3U$ at the distance $\Delta_U^{\max} = 10^3 \delta_U^\nu$ from the upper side of the plate.

The time variation of the pressure scaled to $P_0 = 0.5\rho U^2$ in the flow at different distances from the upper side of the plate are shown in Fig. 8. The complex behavior of the curves at the leading edge reflects the presence of both large and small nonuniformities in the flow, which are simultaneously formed in this region. With increase in time, the small-scale components are damped and the curves are smoothed. The periodic character of the curves makes it possible to calculate the frequencies of the vortices in different flow regions, both over the plate and in the wake behind the plate.

In this flow regime, near the leading edge of the plate the average frequency of oscillations is $\omega_p \approx 52$ Hz, whereas in the wake near the trailing edges the local frequency varies over a fairly wide range below the limiting value of 22 Hz. This agrees with the estimates obtained by comparing the ratios of the phase velocity of the vortex structures and the vortex sizes near the plate surface and in the wake.

The pressure distributions along the upper surface of the plate at the successive instants of time reflect the nonuniformity of the field and the unsteady vortex structure of the flow (Fig. 9). The pressure disturbances grow monotonically with approach to the obstacle, attain the maximum $P_{\max} = 0.6P_0$ at a distance of the

order of the plate thickness from the leading edge, then sharply decrease to the minimum value $P_{\min} = -2.3P_0$ directly at the plate, and then vary nonmonotonically along the plate surface and in the wake.

The dependence of the pressure in the leading disturbance on the distance to the plate at the central plane horizon is approximated by a set of functions in the form: $P_0 \sum_{i=1}^{N} A_i \exp(a_i(x + L/2))$, $x \in (-\infty,\ -L/2)$, where $N = 2$ and $A_1 = 1$, $A_2 = 0.23$, $a_1 = 200$, and $a_2 = 40$ [23]. With increase in the distance from the leading edge of the plate to $L/20$, less than a half of the excess pressure attained directly at the edge is lost.

In the strongly stratified fluid, the oscillations are most well expressed over the first quarter of the plate length and, in the weakly stratified fluid, over the last quarter. This is because the smoothing action of stratification, damping the fluid transport in the vertical direction, stabilizes the location of the vortex layer boundaries and restricts the pressure fluctuation amplitude. In the strongly stratified fluid, the variations of the oscillation frequency are smaller and their amplitude decreases more regularly at the central part of the plate, as compared with the weakly stratified fluid, in which the low-frequency fluctuations are manifested in the wake region (Figs. 9a, 9b).

The distributions of the friction coefficient along the plate surface at different instants of time are compared with the Blasius solution [6] in Fig. 10. The shape of the curves reflect the vortex structure of the flow. Near the leading edge of the plate, intense jumps of the friction coefficient, both positive and negative, are observed.

The integral values of the plate drag coefficient differ on average by a factor of 3.5 from the Blasius theory [6], in which the effects of sharp edges and hence vortex generation are not taken into account. For a thin plate ($h = 0.05$ cm), this difference decreases to 2.3 times. In the numerical modeling of the flow over a semi-infinite plate, the difference does not exceed 5%. With decrease in the thickness of the plate, the flow structure becomes less sensitive to both the direct and indirect action of the buoyancy forces.

4. DISCUSSION OF THE RESULTS

The results presented above continue the study (performed using the same mathematical formulation) of the diffusion-induced flows in a continuously stratified fluid on a fixed horizontal plate [15] and the generation of internal waves by a moving plate of finite length within the linear [17] and full nonlinear approach [23]. The mathematical consistency of the formulations over a wide range of the Reynolds numbers, from Re = 1 to 80000, makes it possible to use the calculations for small Re as the initial conditions in the calculations at large Re, which noticeably reduces the calculation time. The calculations performed for four types of fluids, namely, strongly and weakly stratified and potentially and actually homogeneous, make it possible to analyze the vortex generation mechanisms.

The spatial and temporal analysis of the fundamental system of equations, the initial and boundary conditions of a specific problem makes it possible to formulate the objective criteria of the choice of the cell size, the time step, and to optimize the grid, ensuring the stability of the calculations.

The calculations of stratified flows confirmed the efficiency of the baroclinic mechanism of vortex generation with the rate $\dot{\Omega} = \nabla P \times \nabla(\rho^{-1})$ due to the mutual influence of the noncollinear fields in the regions of large pressure and density gradients.

The unsteadiness of the flow for the fixed boundary conditions is attributable to the interactions of large- and small-scale elements, characterized by their own geometry, spatial and temporal scales, the degree of clearness, and the attenuation rate. The main vortex generation occurs in the neighborhood of the leading edge in the zone of maximal divergence of the flow.

The merging of independent vortex systems in the near wake is accompanied by the decrease in the characteristic frequency of the vortices. In the entire flow region, both the processes of generation and break-up of vorticity remain expressed. In the homogeneous-fluid approximation, the macrostructure of the vortex flow is qualitatively similar to that calculated for stratified fluid; however, the condition of constant density makes difficult the determination of the physical mechanisms of vorticity generation.

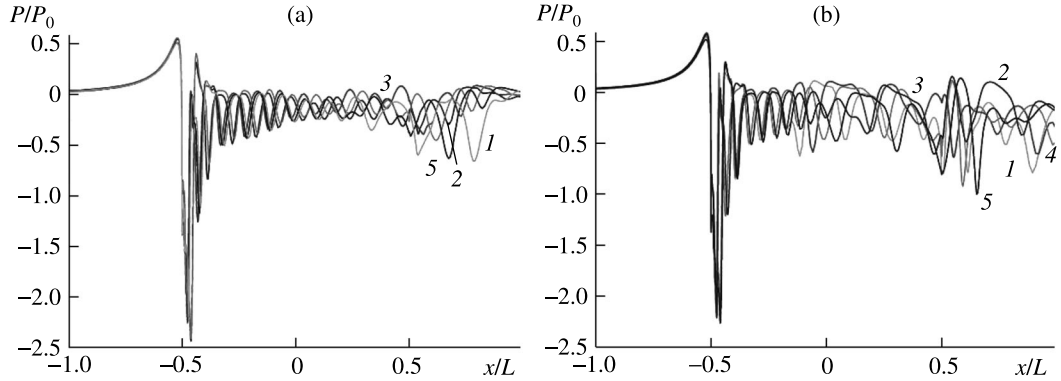

Fig. 9. Distribution of the normalized pressure over the upper surface of the plate ($L = 10$ cm, $h = 0.5$ cm, $U = 80$ cm/s, Re = 80000): (a, b) $N = 1.2$ s^{-1}, 10^{-5}, curves (*1–5*) correspond to the successive instants of time with the step $\Delta T = 0.6/\omega_p$.

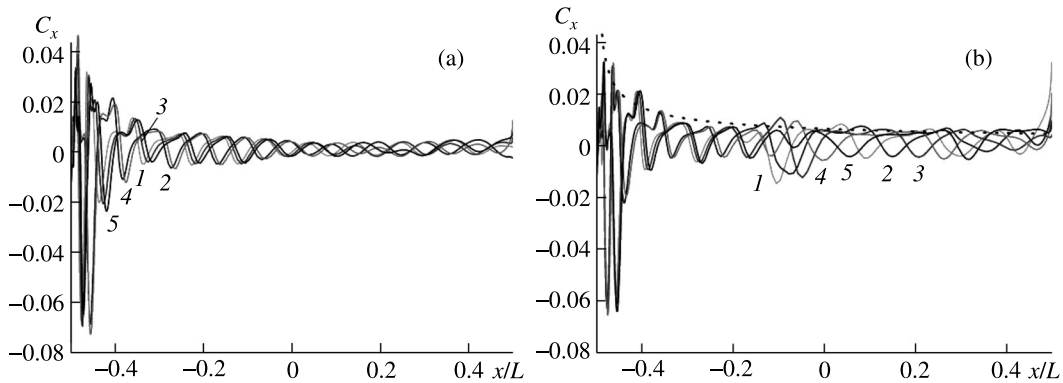

Fig. 10. Distributions of the friction coefficient along the upper surface of the plate ($L = 10$ cm, $h = 0.5$ cm, $U = 80$ cm/s, Re = 80000): (a, b) in the stratified and the actually homogeneous fluid (broken curve shows the Blasius solution [6]), curves (*1–5*) correspond to the successive instants of time with the step $\Delta T = 0.6/\omega_p$.

The calculation results agree qualitatively with the results of visualization of a stratified flow behind a thin plate oriented horizontally or perpendicularly to the free stream [16, 18, 22].

Summary. Using a computer program with open codes a method of constructing a two-dimensional solution of the fundamental system of equations of incompressible weakly and strongly stratified and (potentially and actually) homogeneous fluids is first developed. This method makes it possible to analyze the dynamics and fine structure of flows in a wide range of Reynolds numbers. The comparison of the calculation results for four kinds of fluids (strongly and weakly stratified, potentially and actually homogeneous) made it possible to control independently the calculation accuracy.

The unsteady patterns of the velocity, pressure, density (and their gradients), vorticity, and energy dissipation rate in the flow around a horizontal strip moving uniformly at a zero angle of attack, necessary for determining the forces and torques on the body, are analyzed for $1 < \mathrm{Re} < 10^5$.

The evolution of the individual structural elements is studied, both the general elements for all kinds of fluids and specific for stratified fluids, such as internal waves and thin layers. The physical vortex formation mechanisms in the regions with large pressure and density gradients near the sharp edges are determined and the dynamics of vortex interaction with the outer flow, violating the steady-state nature of the flow, are studied.

The calculation results agree qualitatively with the data of laboratory modeling of stratified flows and, in the limit of the actually homogeneous fluid, with the calculations of an incompressible flow over a semi-infinite plate in the boundary layer approximation.

In the general formulation, the flow around a plate of finite length is a complex physical process which requires a detailed experimental and theoretical study with account for the diffusion, heat conductivity, and compressibility effects, with the control of the criteria of observability and resolution of all flow components with different scales and with account of individual spatial and temporal parameters of measuring tools.

The work received partial financial support from the Central Aerohydrodynamic Institute named after professor N.E. Zhukovskii, the RFBR (project 15-01-09235), and the DMEMCP of RAS (Program IV-4-12 "Dynamics of the formation and interaction of waves and vortices in continua") with the use of the services of the UniHub technological platform of the supercomputer complex of SRCC MSU. The authors are grateful to S.L. Chernyshev for the interest in the work and stimulating discussions.

REFERENCES

1. O. Lilienthal, Die Flugapparate, Algemeine Gesichtspunkte bei deren Herstellung und Anwendung, (Mayer and Müller, Berlin, 1894).
2. W. Wright and O. Wright, "Pioneering Aviation Works of Wright Brothers," http://www.paperlessarchives.com/wright_brothers_papers.html
3. R.E Hanson, H.P. Buckley, and P. Lavoie, "Aerodynamic Optimization of the Flat Plate Leading Edge for Experimental Studies of Laminar and Transitional Boundary Layers," Experiments in Fluids **53** (4), 863–871 (2012).
4. C. Liu, Y. Yan, and P. Lu, "Physics of Turbulence Generation and Sustenance in a Boundary Layer," Computers and Fluids **102**, 353–384 (2014).
5. L. Prandtl, "Über Flüssigkeitsbewegung bei sehr kleiner Reibung," in: *Verhandlungen des III Internationalen Mathematiker-Kongress, Heidelberg, 1904. Leipzig, Germany: Teubner. 1905*, pp. 484–491.
6. H. Schlichting, Boundary Layer Theory (Mc-Graw Hill, New York, 1968).
7. T. Khapko, Y. Duguet, T. Kreilos, et al., "Complexity of Localized Coherent Structures in a Boundary-Layer Flow," Eur. Phys. J. E **37** (4) 1–12 (2014).
8. S. Goldstein, "On Laminar Boundary-Layer Flow Near a Position of Separation," Q. J. Mech. Appl. Math. **1**, 43–69 (1948).
9. V.Ya. Neiland, V.V. Bogolepov, G.N. Dugin, and I.I. Lipatov, Asymptotic Theory of Supersonic Flows of Viscous Gas [in Russian] (Fizmatlit, Moscow, 2004).
10. S. Braun and S. Scheichl, "On Recent Developments in Marginal Separation Theory," Phil. Trans. R. Soc. **A372** (2020), 20130343 (2014).
11. A.M. Gaifullin and A.V. Zubtsov, "Flow past a Plate with a Moving Surface," Fluid Dynamics **44** (4), 540–544 (2009).
12. G.R. Grek, V.V. Kozlov, and V.G. Chernorai, "Hydrodynamic Instability of Boundary Layers and Separated Flows," Advances in Mechanics (1), 52–89 (2006).
13. S.S. Sattarzadeh and J.H.M. Fransson, "Experimental Investigation on the Steady and Unsteady Disturbances in a Flat Plate Boundary Layer," Phys. Fluids **26**, 124103 (2014).
14. Yu.D. Chashechkin, "Differential Mechanics of Fluids: Self-Consistent Analytical, Numerical, and Laboratory Models of Stratified Flows," Bulletin of N.E. Bauman MSTU (6), 67–95 (2014).
15. Ya.V. Zagumennyi and Yu.D. Chashechkin, "Fine Structure of an Unsteady Diffusion-Induced Flow over a Fixed Plate," Fluid Dynamics **48** (3), 374–388 (2013).
16. Yu.D. Chashechkin and V.V. Mitkin, "A Visual Study on Flow Pattern around the Strip Moving Uniformly in a Continuously Stratified Fluid," J. Visualiz. **7** (2), 127–134 (2004).
17. R.N. Bardakov and Yu.D. Chashechkin, "Calculation and Visualization of Two-Dimensional Attached Internal Waves in an Exponentially Stratified Viscous Fluid," Izv. RAS, Fizika Atmos. Okeana **40** (4) 531–544 (2004).
18. R.N. Bardakov, V.V. Mitkin, and Yu.D. Chashechkin, "Fine Structure of a Stratified Flow over a Plate," Prikl. Mekh. Tekh. Fiz. **48** (6), 77–91 (2007).
19. L.D. Landau and E.M. Lifshits, Theoretical Physics. V. 6. Hydromechanics (Pergamon Press, Oxford, 1987).
20. Open Computational Resources, URLs: http://www.openfoam.com, http://www.paraview.org, http://www.salome-platform.org.
21. N.E. Kochin, I.A. Kibel', and N.V. Roze. V. 1, Theoretical Hydromechanics [in Russian] (GITTL, Moscow, 1955).
22. V.E. Prokhorov and Yu.D. Chashechkin, "Visualization and Acoustic Sounding of the Fine Structure of a Stratified Flow behind a Vertical Plate," Fluid Dynamics **48** (6), 722–733 (2013).
23. Yu.D. Chashechkin and Ya.V. Zagumennyi, "Pressure Field Structure on a Plate in a Transitional Flow Regime," Dokl. RAS **461** (1), 39–44 (2015).